



# The effect of cold rolling on age hardening of Cu-3Ti-3Ni-0.5Si alloy

Jia Liu <sup>a</sup>, Xianhui Wang <sup>a,\*</sup>, Jian Chen <sup>b,\*\*</sup>, Jituo Liu <sup>a</sup>

<sup>a</sup> Shaanxi Province Key Laboratory of Electrical Materials and Infiltration Technology, School of Materials Science and Engineering, Xi'an University of Technology, Xi'an, 710048, PR China

<sup>b</sup> School of Materials and Chemical Engineering, Xi'an Technological University, Xi'an, 710021, PR China

## ARTICLE INFO

### Article history:

Received 17 December 2018

Received in revised form

4 May 2019

Accepted 8 May 2019

Available online 9 May 2019

### Keywords:

Cu alloy

Deformation

Age hardening

Precipitation

Electrical conductivity

## ABSTRACT

This study investigates the age hardening behavior of the cold rolled Cu-3Ti-3Ni-0.5Si alloy upon different deformations. The microstructure and the phase composition after precipitation were characterized by X-ray diffraction, optical microscopy, scanning electron microscopy, and transmission electron microscopy, and the electrical conductivity and mechanical properties of the alloy were tested as well. The as-cast Cu-3Ti-3Ni-0.5Si alloy consists of Ni<sub>2</sub>Ti phase, NiTi phase, and Cu matrix, and Ni<sub>2</sub>Si, Ni<sub>3</sub>Si, and Ni<sub>3</sub>Ti phases precipitated from the Cu matrix after aging treatment. TEM analysis shows that Ni<sub>2</sub>Si phase is coherent with the Cu matrix after 50% deformation and aging at 500 °C for 120 min, with an orientation relationship of  $[201]_{\text{Ni}_2\text{Si}} // [11\bar{1}]_{\text{Cu}}$ . However, Ni<sub>2</sub>Si phase loses its coherence with the Cu matrix if the size of the Ni<sub>2</sub>Si phase is above 4.68 nm. Additionally, large deformation promotes most striped precipitates to transform into fine and spherical precipitates, so the appropriate deformation and aging temperature are beneficial for the improvement on the electrical conductivity and hardness. After 90% deformation and aging for 30 min at 500 °C, Cu-3Ti-3Ni-0.5Si alloy has a good combination of tensile strength, elongation, hardness and electrical conductivity, which are 615 MPa, 25.1%, 268 HV and 33.79 % IACS, respectively. The fracture morphology exhibits numerous fine equiaxed dimples with an average size of about 1 μm, and small amounts of large dimples with an average size of about 10 μm, and the assigned failure mechanism of the Cu-3Ti-3Ni-0.5Si alloy is a ductile fracture.

© 2019 Elsevier B.V. All rights reserved.

## 1. Introduction

Copper alloys have attracted extensive attention in the engineering fields that require excellent mechanical properties along with good electrical conductivity, such as conductive lead wires and wires in suspension springs [1–3]. Among Cu alloys, Cu-Be alloys are widely used for electrical components since they possess an adequate balance between mechanical strength and electrical conductivity [4,5]. However, its high production cost and a hazardous influence on human health and environment hinder widespread applications. Subsequently, it is of significance to develop an environmentally friendly substitute for Cu-Be alloys [6–10].

The age-hardenable Cu-Ti alloys containing approximately 1.0–5.0 wt% Ti are regarded as desired substitutes for the expensive

and toxic Cu-Be alloys [11]. So far, extensive research has been performed to elucidate the relationship of phase composition and mechanical properties of the Cu-Ti alloys. Earlier studies [12] showed that Cu-Ti alloys can be strengthened by the spinodal decomposition. Numerous works [13–16] showed that the metastable β'-Cu<sub>4</sub>Ti phase formed during aging enhances the strengthening effect; however, the phase transformation from the metastable and coherent β'-Cu<sub>4</sub>Ti phase to the equilibrium and incoherent Cu<sub>3</sub>Ti phase occurs if the adequate aging temperature or aging time is exceeded, and thus the strength of Cu-Ti alloys substantially decreases. Since the large solubility of Ti solute atoms in the Cu matrix enhances electron scattering, Cu-Ti alloys exhibit poor electrical conductivity, which requires a substantial improvement. One of the approaches in that direction is the addition of appropriate ternary elements that can effectively reduce Ti concentration in the Cu matrix. Besides, the intermetallic compounds formed by these alloying elements can also give an additional strengthening effect, providing the window for improvement of the electrical conductivity with preserved mechanical properties. So far, some authors [17–20] reported on the effect of the

\* Corresponding author.

\*\* Corresponding author.

E-mail addresses: [xhwang693@xaut.edu.cn](mailto:xhwang693@xaut.edu.cn) (X. Wang), [chenjian@xatu.edu.cn](mailto:chenjian@xatu.edu.cn) (J. Chen).

ternary element additions on the electrical conductivity of binary Cu-Ti alloys. Lebreton et al. [17] and Wang et al. [18] revealed that Sn addition improves the electrical conductivity of Cu-Ti alloy due to the presence of  $\text{CuSn}_3\text{Ti}_5$  phase, which reduces the solute Ti content in the Cu matrix. Markandeya et al. [19] found that Cd addition can remarkably increase the mechanical properties of Cu-Ti alloy, without stating the electrical conductivity data. Konno et al. [20] reported 6 times higher electrical conductivity of Cu-3 at.% Ti alloy upon 4 at.% Al addition, but maximal hardness decreased by 35.7%. Additionally, the electrical conductivity of Cu-Ti alloys can also be improved by reducing the content of Ti in the Cu-Ti alloys, while its strength can be enhanced by in-situ formation of ceramic reinforced particles [2,21,22]. Pan et al. [2] prepared Cu matrix composites by mixed acid treatment, molecular-level method, ball milling, and spark plasma sintering (SPS) process, and the composite displays the highest comprehensive performance, such as 131 HV hardness, 345 MPa ultimate tensile strength, 13.8% elongation, and 87.2 %IACS electrical conductivity.

Ni has a strong affinity with Ti to form  $\text{Ni}_3\text{Ti}$  intermetallic compound, and Si atoms could effectively improve the strength of Cu matrix [23–25]; however, no data have been reported on the effect of Ni and Si co-additions on the microstructure and mechanical properties of Cu-Ti alloys.

In the present work, the effect of cold rolling pre-treatment on the age hardening behavior of Cu-3Ti-3Ni-0.5Si alloy was investigated. The microstructure and precipitation phases were characterized, and the mechanical properties and electrical conductivity were determined as well. Our goal in this study is to prepare Cu-3Ti-3Ni-0.5Si alloy with an optimal combination of strength and electrical conductivity, which will surpass the well-known trade-off between these functional properties. In addition, we aim to get an insight into the age hardening behavior and understand the relation of processing parameters and properties of the Cu-3Ti-3Ni-0.5Si alloy.

## 2. Experimental procedures

A Cu-3Ti-3Ni-0.5Si (wt.%) alloy was fabricated by a vacuum induction melting from the raw materials of pure copper, sponge titanium, pure nickel, and pure silicon. The melting of the raw materials was performed in a vacuum induction melting furnace (ZG-25, Jinzhou Electrical Furnace Co., Ltd., China), and an ingot of 100 mm in diameter and 200 mm in height were cast in a water-cooled copper mold. After surface finishing, the as-cast ingot was homogenized at 800 °C for 120 min in an electrical resistance furnace (SK-G10123K, Tianjin Central Electric Furnace Co., Ltd., China). The slices with the dimensions of  $120 \times 50 \times 10$  mm were cut from the ingot by wire electrical discharge machining (CF2258, Yantai LiKai Intelligence Technology Co., Ltd., China). These slices were solubilized at 850 °C for 240 min in the electrical resistance furnace and subsequently quenched in water. Afterward, the specimens were cold-rolled with different extents of deformation, 30%, 50%, 70%, and 90%, and subsequently aged at 500 and 600 °C for different time intervals in the electrical resistance furnace. The specimens were mechanically ground with abrasive papers of different grit sizes and polished with 0.5  $\mu\text{m}$  diamond grinding agent, and finally etched in the solution of 5 g  $\text{FeCl}_3$ , 15 mL HCl and 100 mL distilled water. The phase composition was determined by an X-ray diffractometer (XRD-7000, Shimadzu, Japan) with  $\text{Cu } K_\alpha$  radiation, the scanning speed of  $2^\circ/\text{min}$ , and the scanning range of  $25\text{--}85^\circ$  ( $2\theta$ ). The morphology and the precipitated phases were characterized by an optical microscope (GX71, Olympus, Japan), a scanning electron microscope (Merlin Compact, Zeiss, Germany) equipped with Oxford Instruments HKL channel 5 electron back-scatter diffraction, and a transmission electron microscope (JEM-

3010, JEOL, Japan). EBSD data were acquired at a scanning step size of 0.6  $\mu\text{m}$ . The specimen was tilted  $70^\circ$  for EBSD mapping at an acceleration voltage of 20 kV. The samples for EBSD analysis were mechanically ground by the abrasive paper, polished with 0.5  $\mu\text{m}$  diamond grinding agent, and vibratory polished for 30 min (VibroMet 2, Buehler, USA). The specimens for TEM analysis were cut from the block using a precision saw (Somet 1000, Buehler, USA) and then mechanically polished to obtain 50  $\mu\text{m}$  thick slices. Discs of 3 mm in diameter were punched from these slices and thinned in an ion milling machine (Fischione 1010, Gatan Inc, USA) at 4.5 kV. The transmission electron microscope was used at an operation voltage of 200 kV. The electrical conductivity was measured using an eddy conductivity gauge (FQR-7501, Sitea Instrument Co., Ltd., China) and the hardness was determined by a hardness testing machine (HV-1000, Fangyuan Instrument Co., Ltd., China) at a load of 100 N holding for 10 s, respectively. The elastic modulus and nano-hardness were tested using a Nano Indenter (G200, Agilent, USA) at a load of 50 N. Tensile tests were performed using a universal test machine (HT-2402, Hungta Instrument Co., Ltd., China) at a strain rate of 1 mm/min.

## 3. Results and discussion

### 3.1. Microstructural characterization

Fig. 1 shows the micrographs and elemental mapping results of the as-cast Cu-3Ti-3Ni-0.5Si alloy. As seen from Fig. 1(a)–(b), some primary phases form during the solidification process. The elemental mapping results indicated that these phases are rich in Ti and Ni but depleted in Cu, while Si elements are uniformly distributed in the Cu matrix, Fig. 1(c)–(f). To determine these primary phases, an X-ray diffraction test was performed, and the XRD pattern is presented in Fig. 2. It can be confirmed that the primary phases are  $\text{Ni}_2\text{Ti}$  and  $\text{NiTi}$  intermetallic compounds.

For the Cu-3Ti-3Ni-0.5Si alloy with 50% deformation after aging at 500 and 600 °C for 120 min, the orientation mappings shown in Fig. 3(a)–(b) are inverse pole figures, and their colors are explained by the color keys on the stereographic triangle. The grain size distributions are shown in Fig. 3(c)–(d), and the grain boundary misorientation distributions are given in Fig. 3(e)–(f). At 500 °C, the recrystallization occurs preferentially at the shear band (Fig. 3(a)). However, at 600 °C, the recrystallization is generated at the shear band and inside the grain. Moreover, large amounts of twins are also observed inside the partially recrystallized grains (Fig. 3(b)). As seen from Fig. 3(c)–(d), the grain size of the alloy aging at 600 °C is smaller than that at 500 °C, and this is due to the occurrence of recrystallization inside the grains. In addition, the low angle grain boundary decreases, while the high angle grain boundary increases (Fig. 3(e)–(f)). This can be explained by the previous reports by Huang et al. [26], Humphreys et al. [27] and Daaland et al. [28]. They determined that small-sized subgrains are merged with large-sized subgrains into a grain due to the rotation of subgrain boundaries. This increases the misorientation between the large-sized subgrains and adjacent subgrains, resulting in the formation of the high-angle grain boundary, which further promotes the nucleation of recrystallization.

Fig. 4(a)–(e) are the SEM micrographs of the Cu-3Ti-3Ni-0.5Si alloy with different deformations after aging at 500 °C for 120 min. At 0% deformation, the secondary phase exists in the form of striped shape, whereas its amount decreases after 30% deformation (Fig. 4(a)–(b)). By further increase of deformation, most striped precipitates transform into fine and spherical precipitates, giving rise to the significant decrease of the amount of the striped precipitate (Fig. 4(c)–(e)).

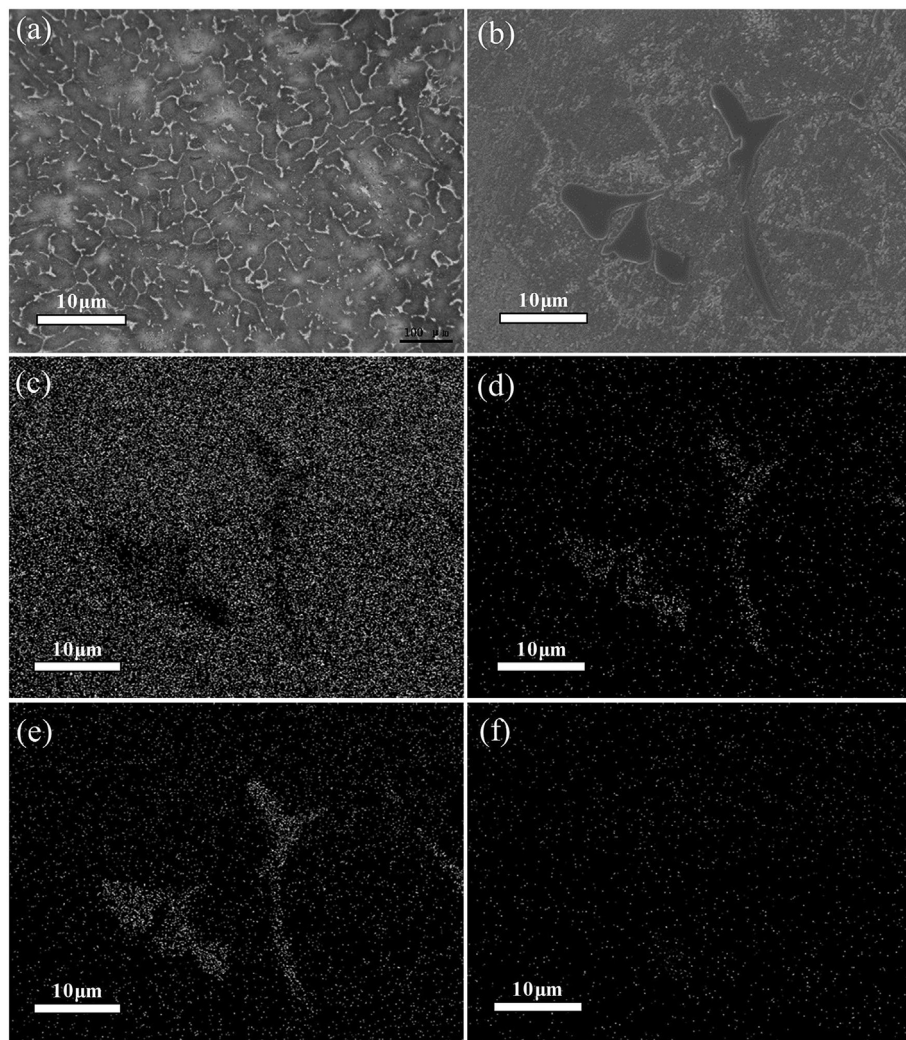


**Fig. 1.** Micrographs and the elemental mapping results of as-cast Cu-3Ti-3Ni-0.5Si alloy: (a) OM image; (b) backscatter electron image; (c) Cu element; (d) Ti element; (e) Ni element; (f) Si element.

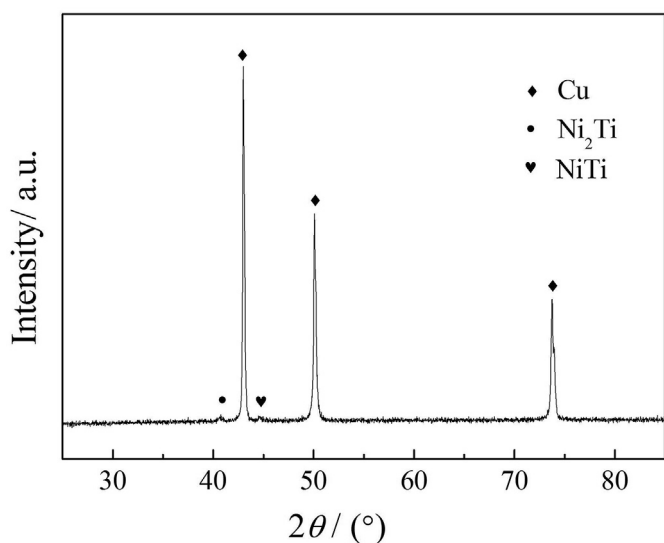


**Fig. 2.** XRD pattern of as-cast Cu-3Ti-3Ni-0.5Si alloy.

### 3.2. TEM characterization

To further determine the phase constituents and clarify the precipitation behavior, TEM analyses were performed on the Cu-3Ti-3Ni-0.5Si alloy with 50% and 90% deformation after aging at 500 °C for 120 min, and the results are shown in Figs. 5–7.

TEM images of the Cu-3Ti-3Ni-0.5Si alloy with 50% deformation after aging at 500 °C for 120 min are shown in Fig. 5(a), (c) and (e), and their corresponding SAED patterns are represented in Fig. 5(b), (d) and (f), respectively. As seen in Fig. 5(a), the precipitate sizes are in the range of 5–10 nm. As determined by the indexed results of the SAED pattern with an electron beam along the zone axis of  $[11\bar{1}]_{\text{Cu}}$  (Fig. 5(b)), it is assumed that the precipitate is  $\text{Ni}_2\text{Si}$ , which has an orthogonal structure with the lattice parameters  $a = 0.499 \text{ nm}$ ,  $b = 0.372 \text{ nm}$ ,  $c = 0.703 \text{ nm}$ ,  $\alpha = 90^\circ$ ,  $\beta = 90^\circ$ ,  $\gamma = 90^\circ$  [23]. In addition, the crystal orientation relationship between  $\text{Ni}_2\text{Si}$  and Cu matrix is  $[\bar{2}01]_{\text{Ni}_2\text{Si}} // [11\bar{1}]_{\text{Cu}}$ . As seen from the insert shown in Fig. 5(a), the interplanar distance of  $\text{Ni}_2\text{Si}$  phase is 0.1118 nm, and the crystal index is (230). The coherent/semi-coherent relation between the precipitate phase and the matrix can be evaluated utilizing their lattice misfit ( $\delta$ ) [29], Eq. (1).



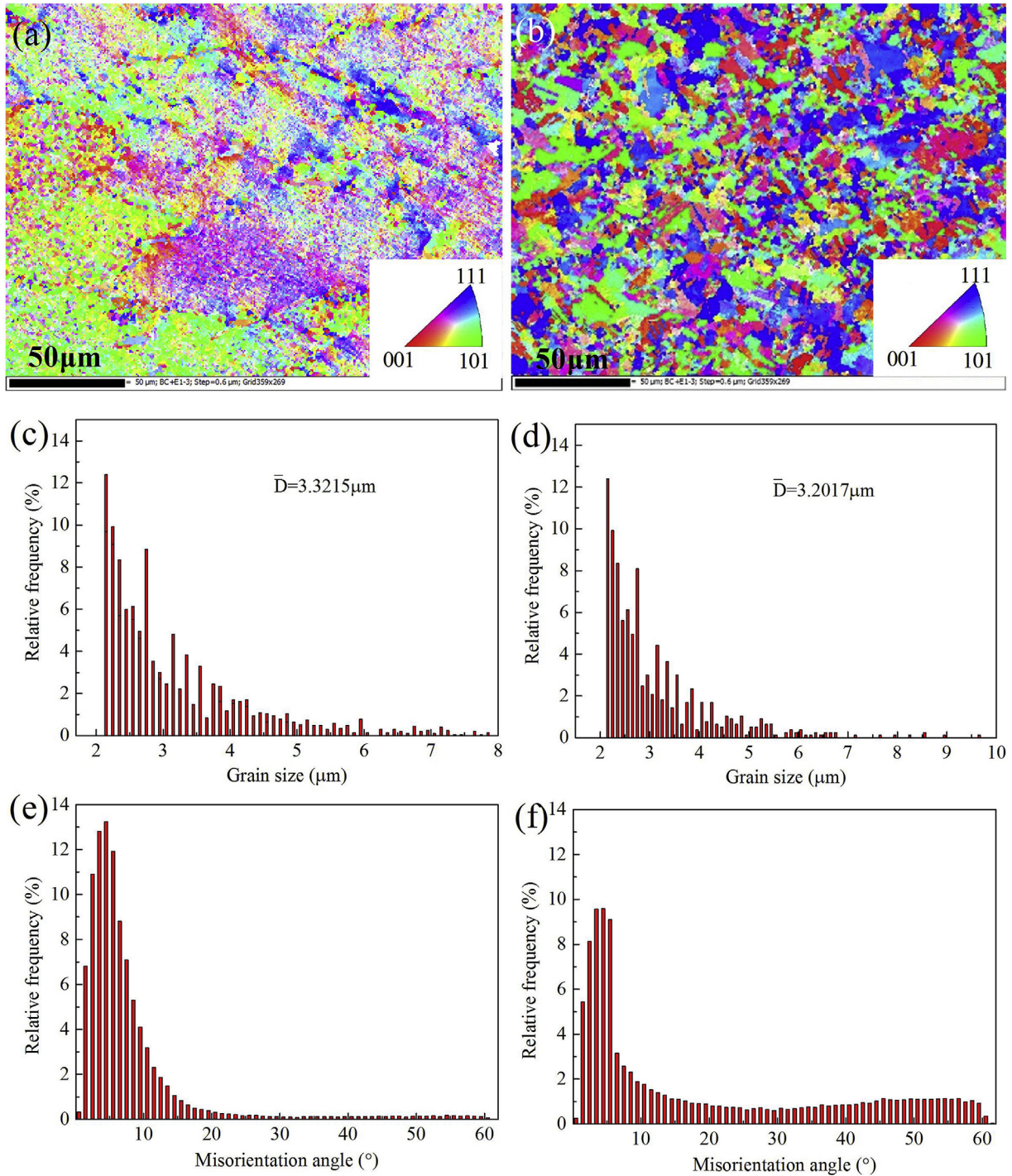


**Fig. 3.** Orientation mappings with the color keys ((a), (b)), grain size distribution ((c), (d)) and grain boundary misorientation distribution ((e), (f)) for the Cu-3Ti-3Ni-0.5Si alloy with 50% deformation after aging for 120 min at 500 °C and 600 °C: (a) (c) (e) 500 °C; (b) (d) (f) 600 °C. (For interpretation of the references to color in this figure legend, the reader is referred to the Web version of this article.)

$$\delta = \frac{2(d_1 - d_2)}{d_1 + d_2} \quad (1)$$

where  $d_1$  and  $d_2$  are the interplanar distances of matrix and precipitate phase.

It is already established that the precipitate phase and matrix phase have a coherent relation if  $\delta$  is less than 0.05. As calculated by Eq. (1), the lattice misfit ( $\delta$ ) between  $\text{Ni}_2\text{Si}$  phase and Cu matrix is

0.025. Hence, it can be concluded that  $\text{Ni}_2\text{Si}$  phase is coherent with the Cu matrix. Generally, the formation of interfacial dislocations is mainly driven by the elastic energy, which is derived from the lattice misfit. If they lose their coherency, the increased interfacial energy by the introduction of dislocations is equal to the decreased elastic energy by the relaxation of lattice distortion. Therefore, the following relationship is valid at a critical radius for the coherent/semi-coherent transition between  $\text{Ni}_2\text{Si}$  phase and Cu matrix. The

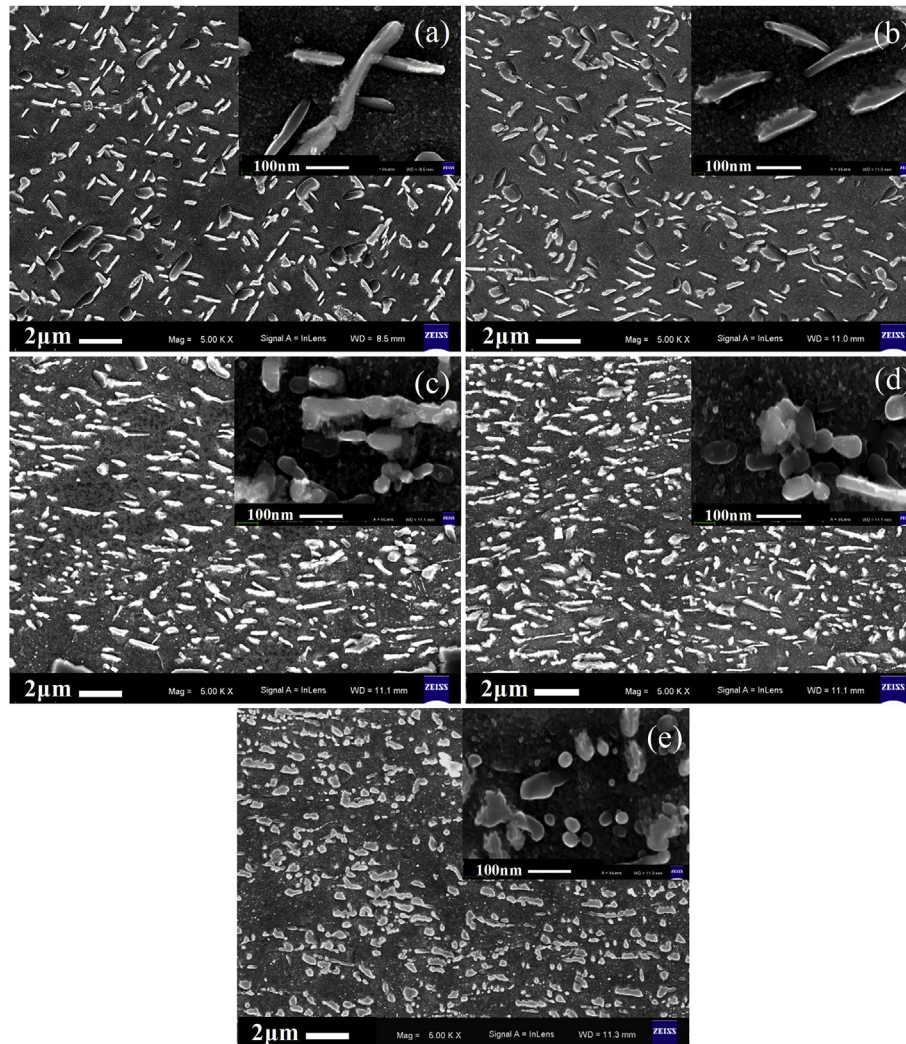


Fig. 4. SEM micrographs of Cu-3Ti-3Ni-0.5Si alloy with different deformations after aging at 500 °C for 120 min: (a) 0%; (b) 30%; (c) 50%; (d) 70%; (e) 90%.

critical radius ( $r$ ) can be calculated by Eqs. (2)–(4) [30].

$$4\pi r^2 \sigma = 8\pi r^3 G \delta^2 \frac{1+\nu}{3(1-\nu)} \quad (2)$$

$$\sigma = \frac{Gb}{2\pi^2} \left\{ 1 + \beta - (1 + \beta^2)^{1/2} - \beta \ln \left[ 2\beta(1 + \beta^2)^{1/2} - 2\beta^2 \right] \right\} \quad (3)$$

$$\beta = \frac{\pi \delta}{1 - \nu} \quad (4)$$

where  $\delta$ ,  $G$ ,  $\nu$ , and  $b$  are lattice misfit, shear modulus, Poisson ratio, and the magnitude of the Burgers vector of Cu, respectively. As determined by the above equations, the critical radius of coherent/semi-coherent transition between  $\text{Ni}_2\text{Si}$  phase and Cu matrix is 4.68 nm. This suggests that their coherency is lost once the size of  $\text{Ni}_2\text{Si}$  phase is beyond 4.68 nm.

It is evident from Fig. 5(c) and (e) that there are the black particle and the striped phase in the Cu matrix. As determined from the indexed results of the SAED pattern with an electron beam along the zone axis of  $[2\bar{4}3]$  (Fig. 5(d)), the black particle is  $\text{Ni}_3\text{Si}$  phase, which has a monoclinic structure with the lattice

parameters  $a = 0.697$  nm,  $b = 0.625$  nm,  $c = 0.507$  nm,  $\alpha = 90^\circ$ ,  $\beta = 132.16^\circ$ ,  $\gamma = 90^\circ$  [25]. As learned from the indexed results of SAED pattern with an electron beam along the zone axis of  $[2\bar{2}0\bar{1}]$  in Fig. 5(f), the black striped phase is  $\text{Ni}_3\text{Ti}$  phase, which has a hexagonal structure with the lattice parameters  $a = 0.5092$  nm,  $b = 0.5092$  nm,  $c = 0.8297$  nm,  $\alpha = 90^\circ$ ,  $\beta = 90^\circ$ ,  $\gamma = 120^\circ$  [31].

Fig. 6(a), (c) and (e) are TEM images of the Cu-3Ti-3Ni-0.5Si alloy with 90% deformation after aging at 500 °C for 120 min, and the corresponding SAED patterns are presented in Fig. 6(b), (d), and (f). It is determined from Fig. 6(a)–(b) that the spherical precipitate is  $\text{Ni}_2\text{Si}$ , and the electron beam direction along the zone axis of the SAED pattern is  $[312]$ . However, as learned from Fig. 6(c)–(d), the particle phase is  $\text{Ni}_3\text{Si}$ , and the electron beam direction along the zone axis of the SAED pattern is  $[2\bar{4}3]$ . Furthermore, Fig. 6(e) shows that the striped and spherical precipitates co-exist in the Cu matrix. As it is evidently shown in Fig. 6(f), the striped precipitate is  $\text{Ni}_3\text{Ti}$  phase and the electron beam direction along the zone axis of the SAED pattern is  $[22\bar{4}3]$ , while the spherical precipitate is  $\text{Ni}_2\text{Si}$  phase, and the electron beam direction along the zone axis of the SAED pattern is  $[11\bar{1}]$ . TEM image and the corresponding SAED patterns (Fig. 7) at three different zones for the Cu-3Ti-3Ni-0.5Si alloy after 90% deformation and aging at 500 °C for 120 min indicate the existence of striped and spherical black precipitates. Both types belong to the  $\text{Ni}_3\text{Ti}$  phase, according to the indexed results of



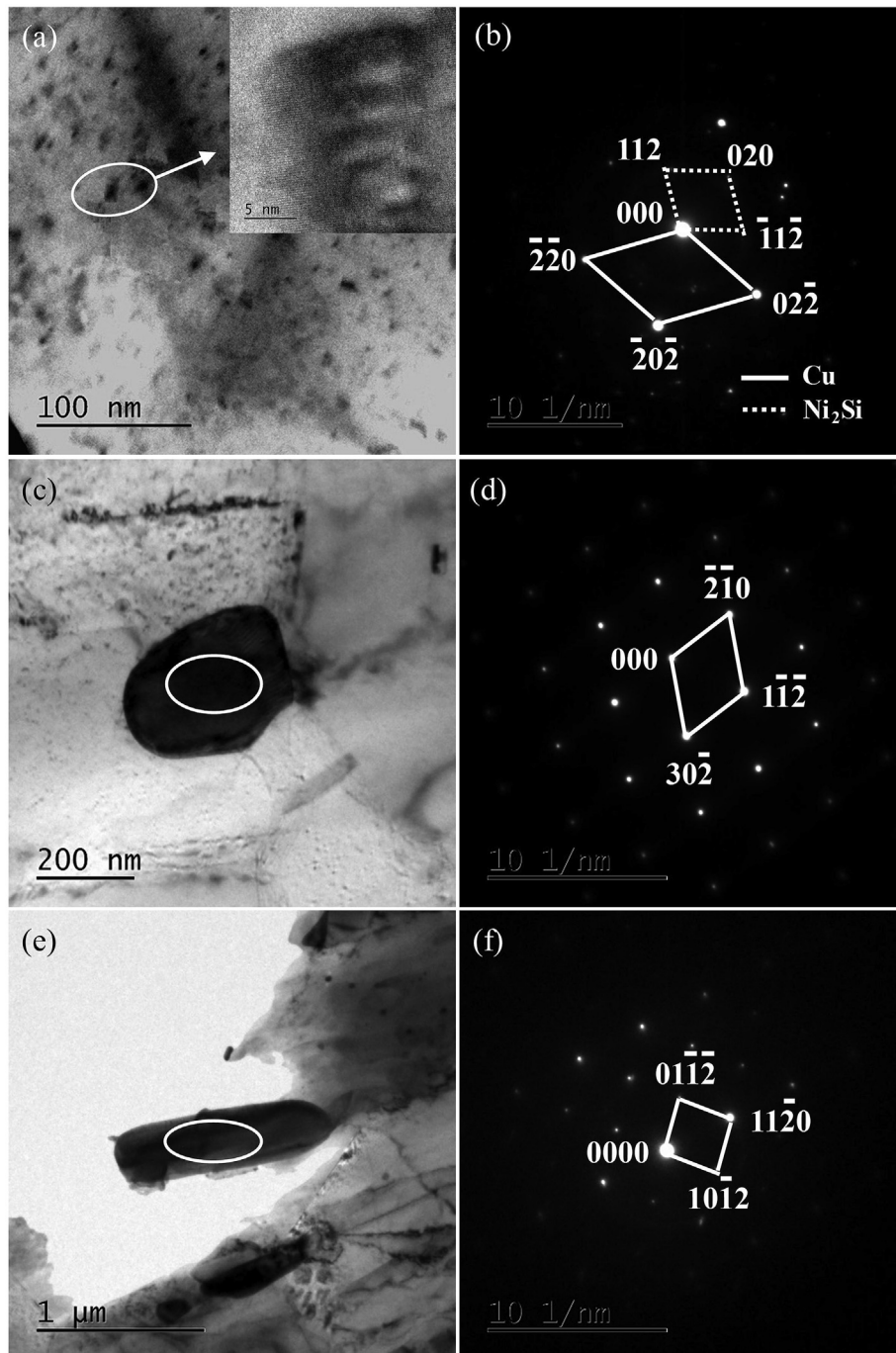


**Fig. 5.** TEM images (a, c, e) and corresponding SAED patterns (b, d, f) of Cu-3Ti-3Ni-0.5Si alloy with 50% deformation after aging at 500 °C for 120 min. The insert is the HRTEM image of elliptical region marked in Fig. 5(a).

SAED patterns with an electron beam along the zone axis of  $[3\bar{3}0\bar{1}]$ .

### 3.3. Mechanical and electrical properties

Fig. 8(a) shows the variation of the hardness with deformation of the Cu-3Ti-3Ni-0.5Si alloy aged for 120 min at different temperatures. At the initial stage of aging, Ti, Ni and Si solute atoms have large supersaturated concentrations in the Cu matrix, which promote the precipitation, and, thus, the concentration of those solute atoms is remarkably reduced once the precipitates form, which is favorable for the increase of hardness. Nevertheless, the

hardness of the alloy aged at 550 °C slightly decreases if the deformation is above 30% in comparison with that at 500 °C. This originates from the precipitate coarsening at higher aging temperature. Fig. 8(b) shows variation in electrical conductivity with deformation for the Cu-3Ti-3Ni-0.5Si alloy aged for 120 min at different temperatures. Apparently, the electrical conductivity increases with deformation and aging temperature. Since the electrical conductivity is more sensitive to solute concentration in the matrix, the precipitation of Ti, Ni, and Si solute atoms reduces the electron scattering [24], and thus, increases the electrical conductivity.

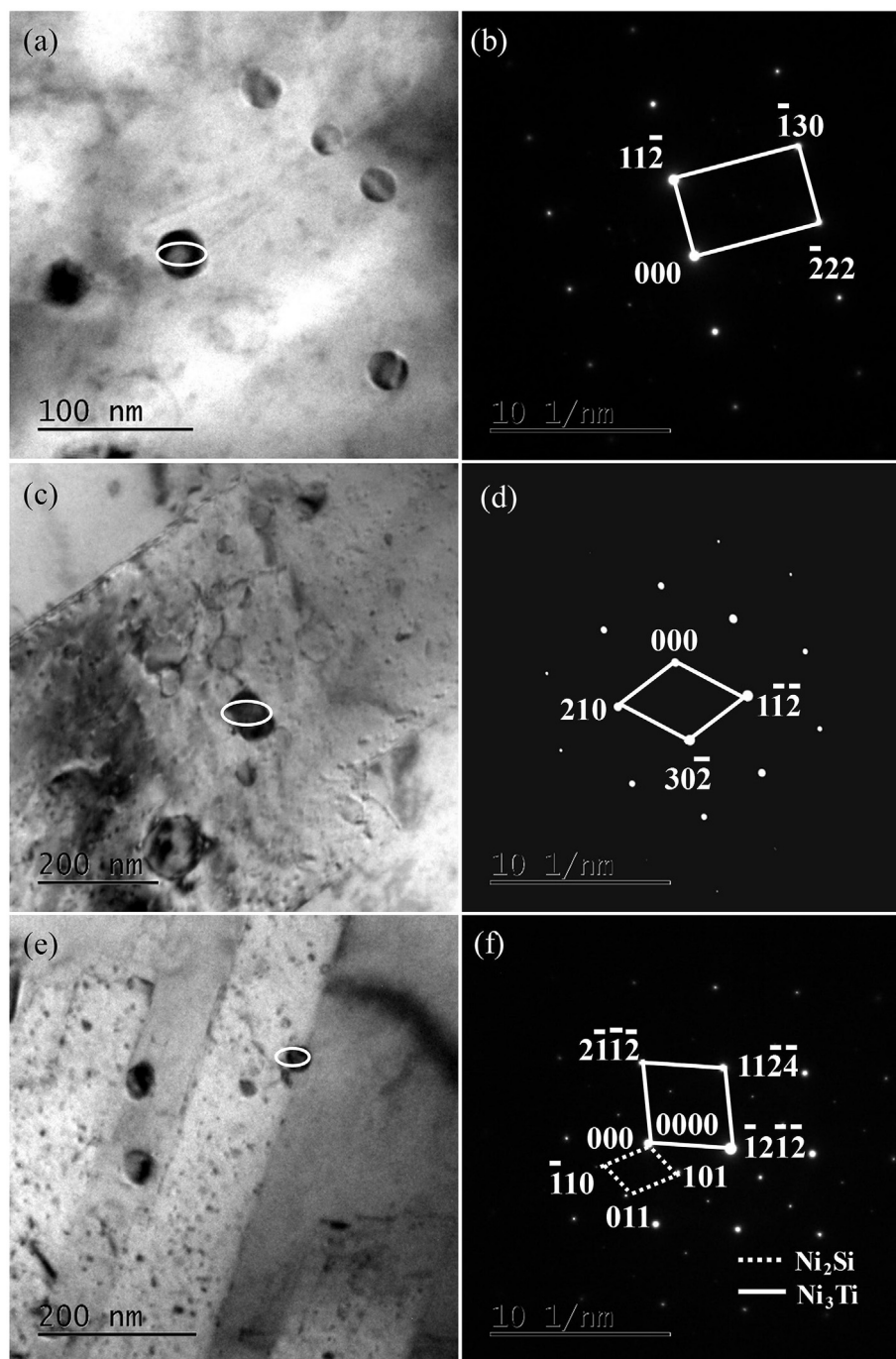


**Fig. 6.** TEM images (a, c, e) and corresponding SAED patterns (b, d, f) of Cu-3Ti-3Ni-0.5Si alloy with 90% deformation after aging at 500 °C for 120 min.

**Fig. 9(a)** shows the dependence of the hardness on aging time for Cu-3Ti-3Ni-0.5Si alloy. The initial sharp increase in hardness increases can be explained by the formation of large numbers of precipitates which yields a significant decrease of Ti, Ni, and Si solute atoms in the Cu matrix, and these precipitates contribute to the increase of the hardness. However, the prolonged aging time causes precipitate coarsening, which progressively reduces the strengthening effect, and, thus, hardness decreases slowly with aging time. The hardness at 90% deformation is slightly lower than that at 70% deformation after peak aging, which can be attributed to the formation of more dislocations during large deformation. Previously was suggested that dislocations promote the nucleation

of recrystallization, while it also causes a decrease in a number of dislocations [27]. Hence, the hardness decreases slightly after large deformation. As discussed above, the strengthening of the Cu-Ti-Ni-Si quaternary alloy is dominated by the precipitation phases, such as  $\text{Ni}_3\text{Ti}$ ,  $\text{Ni}_3\text{Si}$  and  $\text{Ni}_2\text{Si}$ . This differs from the Cu-Ti binary alloy and ternary alloy. For the Cu-Ti binary alloy, the strengthening is mainly derived from the spinodal decomposition and the  $\beta'$ - $\text{Cu}_4\text{Ti}$  phase formation during aging [11,16]. Nevertheless, for the Cu-Ti-Ni alloy [32,33] and Cu-Ti-Al ternary alloy [20], these precipitation phases, such as  $\beta'$ - $\text{Cu}_4\text{Ti}$ ,  $\text{Ni}_3\text{Ti}$  and  $\text{Ti}_3\text{Al}$ , promote the strengthening effect.

**Fig. 9(b)** shows a dependence of the electrical conductivity on

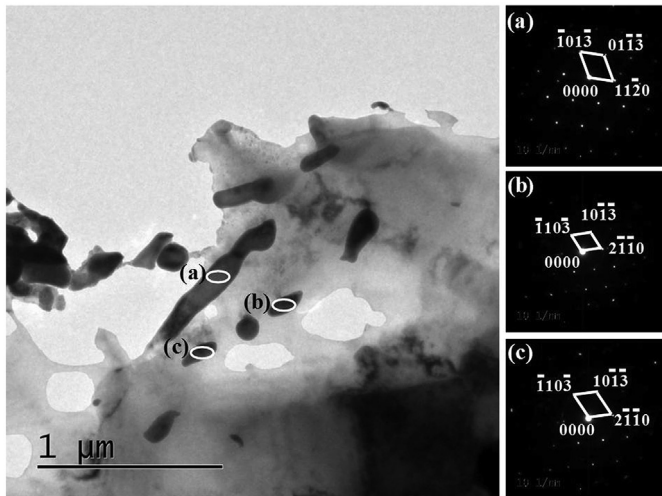


**Fig. 7.** TEM image and corresponding SAED patterns for Cu-3Ti-3Ni-0.5Si alloy with 90% deformation after aging at 500 °C for 120 min.

aging time for the Cu-3Ti-3Ni-0.5Si alloy. The electrical conductivity increases rapidly at the initial stage, with a subsequent progressive increase with aging time. The solute atoms dissolved in the

Cu matrix cause larger electron scattering than those at the grain boundary [34]. At the initial stage of aging, the concentration of Ti, Ni, and Si solute atoms in the Cu matrix is high, with plausible high precipitation rate from the Cu matrix, lowering the concentration of these solute atoms in the Cu matrix. Subsequently, the electrical conductivity sharply increases at the initial stage. However, the concentrations of these solute atoms gradually reduce in the Cu matrix with a further increase of aging time, causing a low precipitation rate and yielding a slight increase of the electrical conductivity.

**Fig. 10(a)** shows representative nanoindentation load-displacement curves of the Cu-3Ti-3Ni-0.5Si alloy with different deformations after aging at 500 °C for 120 min. **Fig. 10(b)** shows the dependence of the elastic modulus and nano-hardness on deformation for the Cu-3Ti-3Ni-0.5Si alloy aged at 500 °C for 120 min. It was determined that the elastic modulus of the Cu-3Ti-3Ni-0.5Si alloy does not change significantly after deformation and aging treatment. This is consistent with the conventional viewpoint [35]. Generally, it is assumed that the elastic modulus of the metallic materials is insensitive to microstructure, cold deformation and heat treatment.

Tensile tests were performed to evaluate the mechanical properties of the differently deformed Cu-3Ti-3Ni-0.5Si alloy after peak aging, and the results are listed in **Table 1**. In order to compare their comprehensive performances, the electrical conductivity is also

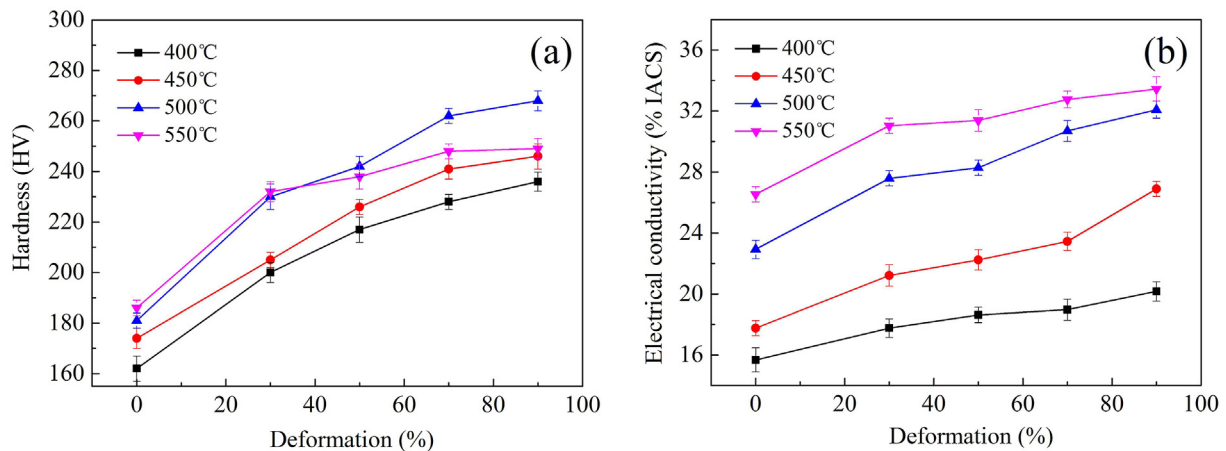


**Fig. 8.** Variation of the hardness (a) and electrical conductivity (b) with deformation for Cu-3Ti-3Ni-0.5Si alloy.

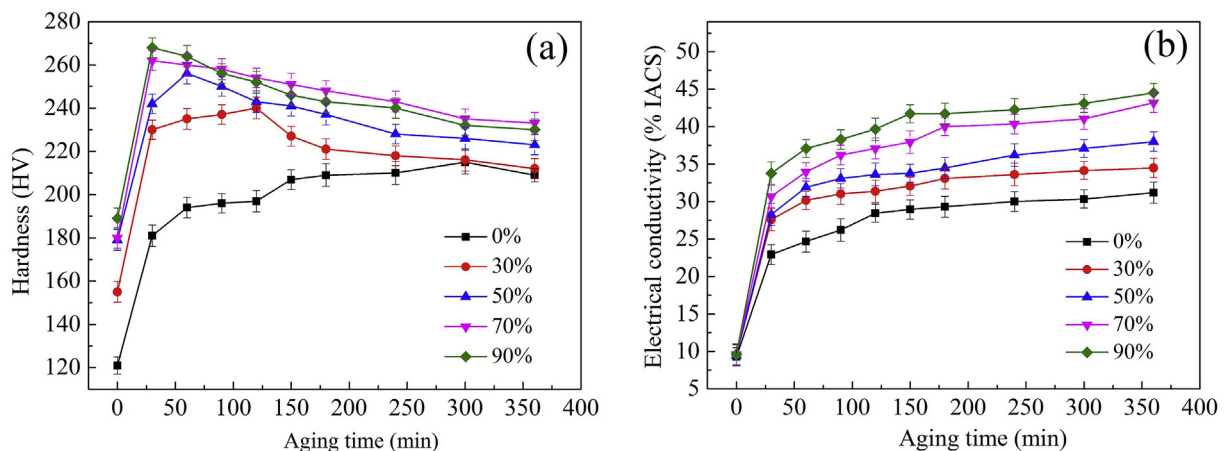


**Fig. 9.** Variation of the hardness (a) and electrical conductivity (b) with aging time for the Cu-3Ti-3Ni-0.5Si alloy.



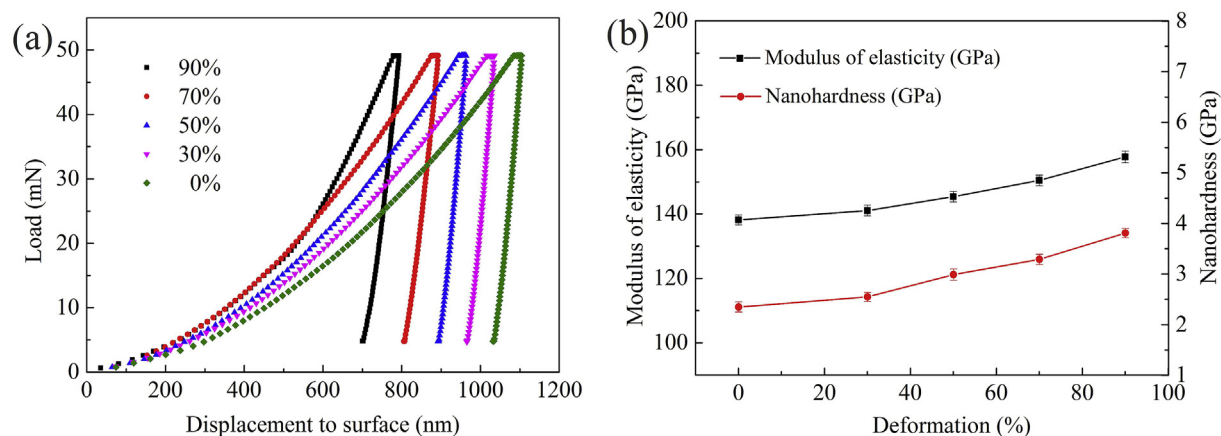


**Fig. 10.** Representative nanoindentation load-displacement curves (a) and the elastic modulus and nano-hardness with dependence of deformation (b) for the Cu-3Ti-3Ni-0.5Si alloy after aging at 500 °C for 120 min.

**Table 1**  
The properties of deformed Cu-3Ti-3Ni-0.5Si alloy peak aged at 500 °C.

Deformation/aging time	TS (MPa)	EL (%)	EC (%IACS)	Hardness (HV)
0%/300 min	518	22.6	30.34	215
30%/120 min	520	28.3	31.38	240
50%/60 min	528	25.7	31.90	256
70%/30 min	546	24.9	30.69	262
90%/30 min	615	25.1	33.79	268

included in Table 1. After aging at 500 °C for 30 min, the Cu-3Ti-3Ni-0.5Si alloy with 90% deformation has a good combination of the tensile strength (TS), elongation (EL), hardness, and electrical conductivity (EC), which are 615 MPa, 25.1%, 268 HV and 33.79% IACS, respectively. Compared with our previous research [32], the hardness value and electrical conductivity of Cu-3Ti-3Ni alloy are increased by 39.9% and 1.79%, respectively. Markandeya et al. [16] reported that the tensile strength, elongation, and hardness of Cu-3Ti-1Cr alloy are 890 MPa, 17%, and 300 HV, respectively. However, there is no stated value of electrical conductivity. Markandeya et al. [19] also studied the Cu-Ti-Cd alloy and determined that Cd addition can significantly enhance tensile strength, which reaches up to 916 MPa, whereas the elongation is decreased to 13%. Similarly, there is on reported data on electrical conductivity. Konno et al. [20] studied the effect of 4 at.% Al addition on the hardness and electrical conductivity of the Cu-3 at.% Ti alloy, and the results indicated

that this ternary alloy has a peak hardness value of 180 HV and electrical conductivity of 6 %IACS. Subsequently, it is suggested that the Cu-3Ti-3Ni-0.5Si alloy has a good combination of electrical conductivity and mechanical properties.

Fig. 11 shows the SEM fracture morphology at different magnifications for the Cu-3Ti-3Ni-0.5Si alloy with 90% deformation after aging at 500 °C for 30 min. Apparently, the fracture morphology exhibits numerous small equiaxed dimples along with some deep and large dimples. As determined from the magnified image of the region marked by a dashed rectangle, these small equiaxed dimples have an average size of about 1 μm, while the average size of deep and large dimples is approximately 10 μm, (Fig. 11(b)). The formation of dimples is derived from the inter-linking of the voids formed during deformation [36,37]. Hence, it is suggested that the failure of the alloy proceeds via a ductile rupture mechanism.

#### 4. Conclusions

- (1) Ni<sub>2</sub>Si, Ni<sub>3</sub>Si, and Ni<sub>3</sub>Ti phases precipitate from the Cu matrix after aging treatment, and they have an orthogonal, monoclinic, and hexagonal crystal structure, respectively.
- (2) For the studied alloy without deformation, the precipitated Ni<sub>3</sub>Ti phase has striped morphology, but it transforms into spherical morphology with an increase of deformation.
- (3) Ni<sub>2</sub>Si precipitation phase is coherent with the Cu matrix after 50% deformation and aging at 500 °C for 120 min, and their orientation relationship is  $[201]_{\text{Ni}_2\text{Si}} // [11\bar{1}]_{\text{Cu}}$ .

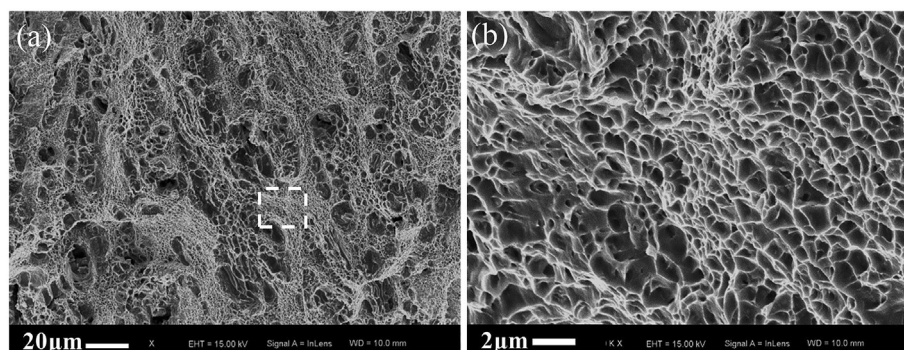


**Fig. 11.** SEM fracture morphology at different magnifications for the Cu-3Ti-3Ni-0.5Si alloy with 90% deformation after aging at 500 °C for 30 min.

- (4) Both electrical conductivity and hardness increase with deformation and aging temperature, but too large deformation and high aging temperature are detrimental to electrical conductivity and hardness.
- (5) In the experimentally investigated range, the Cu-3Ti-3Ni-0.5Si alloy has a good combination of mechanical and electrical properties after cold rolling by 90% and aging treatment at 500 °C for 30 min. The tensile strength, elongation, hardness and electrical conductivity are 615 MPa, 25.1%, 268 HV and 33.79 %IACS, respectively.
- (6) Numerous small equiaxed dimples along with some deep and large dimples are present on the fracture surface. The suggested failure mechanism of Cu-3Ti-3Ni-0.5Si alloy is a ductile fracture.

## Acknowledgements

This research was supported by the National Natural Science Foundation of China (No. 51605146), Key Program of the National Natural Science Foundation of China (U1502274), Research Fund of Shaanxi Key Laboratory of Comprehensive Utilization of Tailings Resources (2017SKY-WK010), and the Special Research Projects of Shaanxi Province Department of Education (18JK0244).

## References

- [1] Z.Q. Zhao, Z. Xiao, Z. Li, M.Z. Ma, J. Dai, Effect of magnesium on microstructure and properties of Cu-Cr alloy, *J. Alloys Compd.* 752 (2018) 191–197.
- [2] Y. Pan, S.Q. Xiao, X. Lu, C. Zhou, Y. Li, Z.W. Liu, B.W. Liu, W. Xu, C.C. Jia, X.H. Qu, Fabrication, mechanical properties and electrical conductivity of Al<sub>2</sub>O<sub>3</sub> reinforced Cu/CNTs composites, *J. Alloys Compd.* 782 (2019) 1015–1023.
- [3] Y.X. Liu, L. Wang, K. Jiang, S.T. Yang, Electro-deposition preparation of self-standing Cu-Sn alloy anode electrode for lithium ion battery, *J. Alloys Compd.* 775 (2019) 818–825.
- [4] Q.M. Liu, L.J. Cheng, Structural evolution and electronic properties of Cu-Zn alloy clusters, *J. Alloys Compd.* 771 (2019) 762–768.
- [5] M.Z. Ma, Z. Li, W.T. Qiu, Z. Xiao, Z.Q. Zhao, Y.B. Jiang, Microstructure and properties of Cu-Mg-Ca alloy processed by equal channel angular pressing, *J. Alloys Compd.* 788 (2019) 50–60.
- [6] Z. Tan, X.Y. Zhang, Z.L. Zhou, Z. Zhou, Y. Yang, X.Y. Guo, Z.J. Wang, X. Wu, G.H. Wang, D.Y. He, Thermal effect on the microstructure of the lattice structure Cu-10Sn alloy fabricated through selective laser melting, *J. Alloys Compd.* 787 (2019) 903–908.
- [7] X.P. Xiao, Z.Y. Yi, T.T. Chen, R.Q. Liu, H. Wang, Suppressing spinodal decomposition by adding Co into Cu-Ni-Si alloy, *J. Alloys Compd.* 660 (2016) 178–183.
- [8] Y.J. Zhou, K.X. Song, J.D. Xing, Y.M. Zhang, Precipitation behavior and properties of aged Cu-0.23Be-0.84Co alloy, *J. Alloys Compd.* 658 (2016) 920–930.
- [9] S. Xu, H.D. Fu, Y.T. Wang, J.X. Xie, Effect of Ag addition on the microstructure and mechanical properties of CuCr alloy, *Mater. Sci. Eng. A* 726 (2018) 208–214.
- [10] Z.K. Guo, J.C. Jie, \*S.C. Liu, Y.B. Zhang, B.L. Qin, T.M. Wang, T.J. Li, Effect of V addition on microstructures and mechanical properties of Cu-15Ni-8Sn alloy, *Mater. Sci. Eng. A* 748 (2019) 85–94.
- [11] S. Suzuki, K. Hirabayashi, H. Shibata, K. Mimura, M. Isshiki, Y. Waseda, Electrical and thermal conductivities in quenched and aged high-purity Cu-Ti alloys, *Scripta Mater.* 48 (2003) 431–435.
- [12] W.A. Soffa, D.E. Laughlin, High-strength age hardening copper-titanium alloys: redivivus, *Prog. Mater. Sci.* 49 (2004) 347–366.
- [13] R. Markandeya, S. Nagarjuna, D.S. Sarma, Effect of prior cold work on age hardening of Cu-4Ti-1Cr alloy, *Mater. Sci. Eng. A* 404 (2005) 305–313.
- [14] S. Kim, M. Kang, Hydrogen production from methanol steam reforming over Cu-Ti-P oxide catalysts, *J. Ind. Eng. Chem.* 18 (2012) 969–978.
- [15] S. Nagarajuna, K. Balasubramanian, D.S. Sarma, Effect of Ti additions on the electrical resistivity of copper, *Mater. Sci. Eng. A* 225 (1997) 118–124.
- [16] R. Markandeya, S. Nagarjuna, D.S. Sarma, Effect of prior cold work on age hardening of Cu-3Ti-1Cr alloy, *Mater. Char.* 57 (2006) 348–357.
- [17] V. Lebreton, D. Pachoutinski, Y. Bienvenu, An investigation of microstructure and mechanical properties in Cu-Ti-Sn alloys rich in copper, *Mater. Sci. Eng. A* 508 (2009) 83–92.
- [18] X.H. Wang, C.Y. Chen, T.T. Guo, J.T. Zou, X.H. Yang, Microstructure and properties of ternary Cu-Ti-Sn alloy, *J. Mater. Eng. Perform.* 24 (2015) 2738–2743.
- [19] R. Markandeya, S. Nagarjuna, D.S. Sarma, Characterization of prior cold worked and age hardened Cu-3Ti-1Cd alloy, *Mater. Char.* 54 (2005) 360–369.
- [20] T.J. Konno, R. Nishio, S. Semboshi, T. Ohsumi, E. Okunishi, Aging behavior of Cu-Ti-Al alloy observed by transmission electron microscopy, *J. Mater. Sci.* 43 (2008) 3761–3768.
- [21] M. Sobhani, A. Mirhabibi, H. Arabi, R.M.D. Brydson, Effects of in situ formation of TiB<sub>2</sub> particles on age hardening behavior of Cu-1 wt% Ti-1 wt% TiB<sub>2</sub>, *Mater. Sci. Eng. A* 577 (2013) 16–22.
- [22] J.Q. Ren, S.H. Liang, Y.H. Jiang, X. Du, Research on microstructure and properties of in situ (TiB<sub>2</sub>-TiB)/Cu composites, *Acta Metall. Sin.* 55 (2019) 126–132.
- [23] W.H. Sun, H.H. Xu, S.H. Liu, Y. Du, Z.H. Yuan, B.Y. Huang, Phase equilibria of the Cu-Ni-Si system at 700 °C, *J. Alloys Compd.* 509 (2011) 9776–9781.
- [24] Q. Lei, Z. Li, C. Dai, J. Wang, X. Chen, J.M. Xie, W.W. Yang, D.L. Chen, Effect of aluminum on microstructure and property of Cu-Ni-Si alloys, *Mater. Sci. Eng. A* 572 (2013) 65–74.
- [25] S.J. Zhang, R.G. Li, H.J. Kang, Z.N. Chen, W. Wang, C.L. Zou, T.J. Li, T.M. Wang, A high strength and high electrical conductivity Cu-Cr-Zr alloy fabricated by cryorolling and intermediate aging treatment, *Mater. Sci. Eng. A* 680 (2017) 108–114.
- [26] K. Huang, K. Marthinsen, Q.L. Zhao, R.E. Logé, The double-edge effect of second-phase particles on the recrystallization behaviour and associated mechanical properties of metallic materials, *Prog. Mater. Sci.* 92 (2018) 284–359.
- [27] F.J. Humphreys, M. Hatherly, Recrystallization and Related Annealing Phenomena, second ed., Pergamon Press, Oxford, 2004.
- [28] O. Daaland, E. Nes, Recrystallization texture development in commercial Al-Mn-Mg alloys, *Acta Mater.* 44 (1996) 1413–1435.
- [29] S.P. Lin, H. Huang, S.P. Wen, Z.R. Nie, TEM observation of the Al<sub>3</sub>Er phase during homogenizing of the 5083 alloy with Er addition, *Acta Metall. Sin.* 45 (2009) 978–982.
- [30] S. Iwamura, Y. Miura, Loss in coherency and coarsening behavior of Al<sub>3</sub>Sc precipitates, *Acta Mater.* 52 (2004) 591–600.
- [31] H. Yoon-Uk, T. Masaki, F. Kazuo, L. Hu-Chul Lee, Transformation of DO<sub>24</sub> η-Ni<sub>3</sub>Ti phase to face-centered cubic austenite during isothermal aging of an Fe-Ni-Ti alloy, *Acta Mater.* 57 (2009) 1176–1187.
- [32] J. Liu, X.H. Wang, T.T. Guo, J.T. Zou, X.H. Yang, Microstructural evolution and properties of aged Cu-3Ti-3Ni alloy, *Rare Metal Mater. Eng.* 45 (2016) 1162–1167.
- [33] J. Liu, X.H. Wang, T.T. Guo, J.T. Zou, X.H. Yang, Microstructure and properties of Cu-Ti-Ni alloys, *Int. J. Miner. Met. Mater.* 22 (2015) 1199–1204.
- [34] Q. Lei, Z. Li, T. Xiao, Y. Pang, Z.Q. Xiang, W.T. Qiu, Z. Xiao, A new ultrahigh strength Cu-Ni-Si alloy, *Intermetallics* 42 (2013) 77–84.
- [35] K. Fujiwara, H. Tanimoto, H. Mizubayashi, Elasticity study of very thin Cu films, *Mater. Sci. Eng. A* 442 (2006) 336–341.
- [36] S. Nagarjuna, M. Srinivas, K. Balasubramanian, D.S. Sarma, The alloy content and grain size dependence of flow stress in Cu-Ti alloys, *Acta Mater.* 44 (1996) 2285–2293.
- [37] S. Nagarjuna, M. Srinivas, K. Balasubramanian, D.S. Sarma, On the variation of mechanical properties with solute content in Cu-Ti alloys, *Mater. Sci. Eng. A* 259 (1999) 34–42.